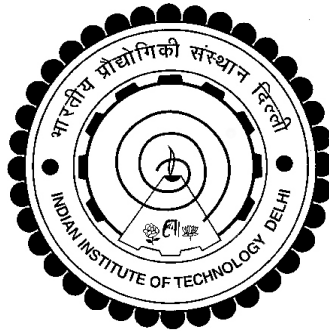


**STUDY OF SPATIO-TEMPORAL EVOLUTION
AND FREQUENCY SHIFTING OF LASER CARRYING
ORBITAL ANGULAR MOMENTUM IN PLASMA**

SUBHAJIT BHASKAR



**DEPARTMENT OF PHYSICS
INDIAN INSTITUTE OF TECHNOLOGY DELHI**

July 2025

© **Indian Institute of Technology Delhi, New Delhi 2025**

**Study of Spatio-Temporal Evolution and Frequency
Shifting of Laser Carrying Orbital Angular Momentum in
Plasma**

by

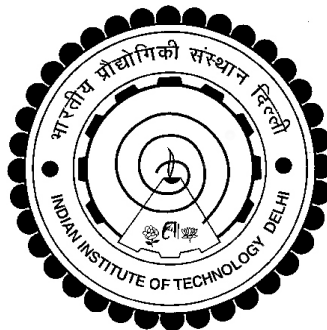
SUBHAJIT BHASKAR

Department of Physics

Submitted

in fulfillment of the requirements of the degree of Doctor of Philosophy

to the



INDIAN INSTITUTE OF TECHNOLOGY DELHI

July 2025

*Dedicated to
my family and loved ones
&
those whoever
inspired and encouraged me*

Certificate

This is to certify that the thesis entitled “**Study of Spatio-Temporal Evolution and Frequency Shifting of Laser Carrying Orbital Angular Momentum in Plasma**” being submitted by **Mr. Subhajt Bhaskar** is worthy of consideration for the award of the degree of Doctor of Philosophy and is a record of the original bonafide research work carried out by him under my guidance and supervision, and that the results contained in it have not been submitted in part or full to any other university or institute for award of any degree / diploma.

I certify that he has pursued the prescribed course of research. I approve the thesis for the award of the degree of Doctor of Philosophy.

Hitendra K. Malik

Professor

Department of Physics

Indian Institute of Technology Delhi

INDIA

Acknowledgements

At the final completion of the thesis, I must first thank God, the All-Powerful, who has given me innumerable blessings, insights, and opportunities. This work would not have been possible without invaluable guidance and support of my supervisor, **Prof. Hitendra K. Malik**. I am extremely appreciative that he accepted me as a student and kept believing in me throughout the years. His depth of expertise and diligent editing have been a huge help to me. My willingness to publish my research work in its current shape was made possible by his unconditional support, invaluable inputs, patience, and cooperation. His long experience, guidance and editing enhanced this research work beyond my expectations.

Thank you to *Prof. R. K. Varshney*, *Prof. Rahul Marathe*, and *Prof. Mayank Kumar*, members of my SRC. Their supportive remarks and insightful, comprehensive feedback mean a lot to me. Furthermore, I am deeply grateful to my M.Sc. mentor *Prof. Surendra Prasad* for the motivation and encouragement during my M.Sc. that helped me get to where I am today.

My PST & PWAPA lab mates Dr. Rajat Dhawan, Dr. Sonu Kumar, Dr. Sandeep Kumar, Dr. Rashmi Shrivastava, Dr. Sheetal Punia, Dr. Manish Dwivedi, Dr. Tamanna Punia, Dhananjay Verma, Rakesh Kumar, Mohit Kumar, Yetendra Prasad Jha, Gaurav Kumar, Deepak Kumar, Shailash Kumar Verma, Shivam Dubey, Amit Kumar and Anupam Shaw who were always willing to assist with any questions I had, deserve special recognition.

I would also like to express special thanks to my friends for being there for me and providing support throughout the challenging times. They have made my time at IITD not only enjoyable but also an educational experience.

Above all, I will always be grateful to my family for their unparalleled love and support, which has been the foundation of my strength and perseverance. To my maa baba, *Smt. Maya Bhaskar and Shri Ranjit Bhaskar*, thank you for teaching me the value of hard work, dedication, and humbleness. Thank you for teaching me how to maintain patience in difficult situations. Your sacrifices and constant trust in my abilities have been the driving force behind all my accomplishments. To my elder brother, *Mr. Avijit Bhaskar*, thank you for encouraging and trusting me. You have always been my back support, and my strength. I want to thank my sister-in-law *Ms. Sanjukta Sarkar* for being there as a sister and supporting and motivating me. A special mention goes to my wife *Ms. Prajna Jyoti Das*, whose patience, understanding, and constant

encouragement have been my pillar of strength. Thank you for standing by me through the ups and downs of this journey and for believing in me even when I doubted myself. To my extended family, my parents in laws, thank you for your prayers, words of encouragement, and love, which have always given me the confidence to push forward. This Ph.D. is not just a personal milestone, but a collective achievement shared with all of you.

I acknowledge the financial support from Ministry of Education, Govt. of India, and Indian Institute of Technology Delhi.

Finally, I would like to dedicate this thesis to the Almighty God and my beloved family.

Subhajit Bhaskar.

Subhajit Bhaskar

Abstract

From development of the very first 100-Watt laser to today's 100 petawatts lasers, e.g., Texas Petawatt laser, Vulcan laser, etc., scientists have enabled us to achieve ultrahigh and ultrashort lasers, and this has opened many domains to research such as higher harmonic generation (HHG), laser wake-field acceleration (LWFA), multiphoton imaging, material processing, ultrafast optical fiber communications, optical manipulations and so on. When an ultra-intense laser passes through a plasma medium, it leads to different nonlinear phenomena, such as Stimulated Raman Scattering (SRS), self-focusing, self-compression, frequency shifting, filamentations, two-plasmon decay, Rayleigh-Taylor instability and so on. Different nonlinearities, like relativistic, ponderomotive, and collisional nonlinearities, are responsible, depending on the time scale, plasma density and laser intensity, for these phenomena to occur in the laser-plasma interaction. Relativistic nonlinearity appears instantaneously ($\tau < \omega_{pe}^{-1}$) when the electron oscillation velocity is of relativistic order. This causes the electron mass to increase. Again, when the laser has an intensity gradient, the plasma particles experience a ponderomotive force in the outward direction from a higher intensity to a lower intensity region. The characteristic time scale for this nonlinearity is $\omega_{pe}^{-1} < \tau < \omega_{pi}^{-1}$, whereas collisional nonlinearity appears at $\tau \sim \omega_{pi}^{-1}$. The nonuniform heating of the plasma electrons leads to temperature inhomogeneity in the medium, and the hotter electrons lose their energy through collisions with the neutral particles. Relativistic mass increase and plasma density modification due to ponderomotive and collisional nonlinearity result in a change in the refractive index and, consequently, the dielectric constant. This causes nonlinear phenomena like self-focusing, defocusing, compression, and stretching to occur. Additionally, the increase in relativistic mass leads to the phenomenon of relativistic self-phase modulation, which in turn causes frequency shifting of the laser. Stimulated Raman Scattering is observed when the plasma density is less than the $\frac{n_{cr}}{4}$. Numerous techniques for examining nonlinear dynamics in a medium are found in the literature, including numerical and molecular simulations. Though the self-focusing phenomenon has a lot of applications starting from high intensity concentration, laser machining, longer propagation distance, plasma generation and filamentation to optical tweezers and micro manipulation, there are several drawbacks such as it can damage the optical components, and induction of thermal effects in the medium can also lead

to unwanted refractive index changes or material deformation, which can hinder precision applications. Therefore, understanding and managing self-focusing is essential for optimizing laser systems in scientific, industrial, and technological applications.

Orbital angular momentum (OAM), which is a form of angular momentum carried by a monochromatic electromagnetic beam, is found to be of central interest to recent researchers because it has given a new degree of freedom in the investigation of the above-mentioned phenomena. It was discovered that electromagnetic beams can have OAM along with the spin angular momentum (SAM) if the phase fronts are helical in nature. Laguerre–Gaussian beams (LG_{pl}), which have helical phase fronts $exp(il\phi)$, consist of two indices: l and p , where the radial index (p) specifies that when OAM (l) is zero, they exhibit p number of rings around the central dot and for non-zero OAM there are $(p + 1)$ number of concentric rings. ϕ is the azimuthal angle that shows self-healing properties as a Bessel–Gaussian beam does under similar conditions but propagates further than them.

Numerous studies exist in literature regarding the above phenomena. However, the majority of them are associated with lasers that do not contain OAM, such as Gaussian, super-Gaussian, and q-Gaussian lasers. The super-Gaussian laser beams have been found to suffer more diffraction divergence than the Gaussian beams in tunnel ionized gases. The literature also indicates that some research has addressed Bessel-Gaussian beams and Laguerre-Gaussian beams. It has been observed that the Laguerre-Gaussian beams can propagate further than the Bessel beams and show more robustness under similar initial conditions. However, these studies primarily focus on spatial evolution and consider only one type of nonlinearity. Also, the spatio-temporal evolution of the LG laser has not been discussed, which gives an inner view of the pulse intensity and phase variation as it propagates through the plasma medium.

In this thesis we have investigated the propagation characteristics of the spatio-temporal evolution of laser carrying orbital angular momentum in underdense plasma and explained the effects of OAM of the laser on the self-focusing and self-compression of the pulse. Effects of the simultaneous presence of relativistic and ponderomotive nonlinearities on the evolution of the spatial profile of LG laser are studied in the initial part of the work. Then, we investigated the spatio-temporal evolution of the LG laser considering only relativistic nonlinearity. Finally, we focused on the relativistic frequency shifting of the LG laser in unmagnetized and magnetized plasmas, respectively. As mathematical model here we have considered the WKB approach to

solve the wave equation then using slowly varying envelope (SVE) approximation and eikonalisation, we have derived the differential equations for the laser beam width and pulse duration. We have also derived the condition where the different nonlinearities cancel each other, and the laser pulse maintains its shape while propagating through the medium. Then the differential equations are solved numerically using Runge-Kutta 4th order method employing MATLAB software. The results are plotted for different numerical parameters and studied variations in the behaviour of curves.

सार

पहले 100-वाट लेज़र के विकास से लेकर आज के 100 पेटावाट लेज़रों, जैसे कि टेक्सास पेटावाट लेज़र, वल्कन लेज़र आदि, वैज्ञानिकों ने हमें अति उच्च और अति लघु लेज़रों को हासिल करने में सक्षम बनाया है, इससे अनुसंधान के कई नए क्षेत्र खुले हैं, जैसे कि उच्च हार्मोनिक उत्पादन (HHG), लेज़र वेक-फील्ड त्वरण (LWFA), बहु-फोटॉन प्रतिरूपण, पदार्थ प्रसंस्करण, अति तीव्र प्रकाशित तंतु संचार, प्रकाशीय मैनिपुलेशन आदि। जब एक अति तीव्र लेज़र प्लाज्मा माध्यम से गुजरता है, तो यह विभिन्न गैर-रेखीय घटनाओं का कारण बनता है, जैसे कि प्रेरित रमन प्रकीर्णन (SRS), स्व-केन्द्रन, स्व-संपीड़न, आवृत्ति स्थानांतरण, तंतुकरण, द्वि-प्लाज़्मोन क्षय, रेले टेलर अस्थिरता आदि। लेजर-प्लाज्मा अंतः क्रिया में इन घटनाओं के घटित होने के लिए विभिन्न अरैखिकताएं, जैसे सापेक्षतावादी, पॉंडरोमोटिव और टकराव संबंधी अरैखिकताएं, समय पैमाने, प्लाज्मा घनत्व और लेजर तीव्रता पर निर्भर करती हैं। सापेक्षतावादी अरैखिकता तत्काल प्रकट होती है ($\tau < \omega_{pe}^{-1}$) जब इलेक्ट्रॉन दोलन वेग सापेक्षतावादी क्रम का होता है। इससे इलेक्ट्रॉन द्रव्यमान में वृद्धि होती है। फिर से, जब लेजर में तीव्रता प्रवणता होती है, तो प्लाज्मा कण उच्च तीव्रता से कम तीव्रता वाले क्षेत्र में बाहरी दिशा में एक पॉंडरोमोटिव बल का अनुभव करते हैं। इस अरैखिकता के लिए विशिष्ट समय पैमाना $\omega_{pe}^{-1} < \tau < \omega_{pi}^{-1}$ है। जबकि टकराव संबंधी अरैखिकता $\tau \sim \omega_{pi}^{-1}$ पर दिखाई देती है। प्लाज्मा इलेक्ट्रॉनों के असमान तापन से माध्यम में तापमान में असमानता आती है, और गर्म इलेक्ट्रॉन तटस्थ कणों के साथ टकराव के माध्यम से अपनी ऊर्जा खो देते हैं। सापेक्षिक द्रव्यमान वृद्धि और पॉंडरोमोटिव तथा टकराव संबंधी अरैखिकता के कारण प्लाज़्मा घनत्व में परिवर्तन के परिणामस्वरूप अपवर्तक सूचकांक में परिवर्तन होता है और परिणामस्वरूप, परावैद्युत स्थिरांक में भी परिवर्तन होता है। इसके कारण स्व-केन्द्रन, डीफोकसिंग, संपीड़न और खिंचाव जैसी अरैखिक घटनाएँ घटित होती हैं। इसके अतिरिक्त, सापेक्षिक द्रव्यमान में वृद्धि सापेक्षिक स्व-चरण मॉड्यूलेशन की घटना को जन्म देती है, जो बदले में लेजर की आवृत्ति में बदलाव का कारण बनती है। उत्तेजित रमन प्रकीर्णन तब देखा जाता है जब प्लाज़्मा घनत्व $n_{cr}/4$ से कम होता है। किसी माध्यम में गैर-रेखीय गतिशीलता की जांच करने के लिए कई तकनीकें साहित्य में पाई जाती हैं, जिनमें संख्यात्मक और आणविक सिमुलेशन शामिल हैं। हालाँकि स्व-केन्द्रन घटना में उच्च तीव्रता सांद्रता, लेजर मशीनिंग, लंबी प्रसार दूरी, प्लाज्मा उत्पादन और तंतुकरण से लेकर प्रकाशिक चिमटी और सूक्ष्म हेरफेर तक कई अनुप्रयोग हैं, लेकिन इसमें कई कमियाँ हैं जैसे कि यह प्रकाशिक घटकों को नुकसान पहुँचा सकता

है, और माध्यम में तापीय प्रभावों के प्रेरण से अवांछित अपवर्तक सूचकांक परिवर्तन या पदार्थ विरूपण भी हो सकता है, जो सटीक अनुप्रयोगों में बाधा उत्पन्न कर सकता है। इसलिए, वैज्ञानिक, औद्योगिक और तकनीकी अनुप्रयोगों में लेजर सिस्टम को अनुकूलित करने के लिए स्व-केन्द्रन को समझना और प्रबंधित करना आवश्यक है।

कक्षीय कोणीय गति (OAM), जो एक एकवर्णी विद्युत-चुम्बकीय किरण द्वारा वहन की जाने वाली कोणीय गति का एक रूप है, हाल के शोधकर्ताओं के लिए केंद्रीय रुचि का विषय पाया गया है क्योंकि इसने उपर्युक्त घटनाओं की जांच में नई स्वतंत्रता की कोटि दी है। यह पता चला कि विद्युत चुम्बकीय किरणों में चक्रण कोणीय गति (SAM) के साथ OAM भी हो सकता है यदि चरणाग्र प्रकृति में कुंडलित हैं। लैगुएरे-गॉसियन किरण (LG_{pl}), जिसमें कुंडलित चरणाग्र $exp(il\phi)$ होते हैं, में दो निर्देशांक होते हैं: l और p , जहां त्रिज्यक निर्देशांक (p) निर्दिष्ट करता है कि जब OAM (l) शून्य होता है, तो वे केंद्रीय बिंदु के चारों ओर p संख्या में रिंग प्रदर्शित करते हैं और गैर-शून्य OAM के लिए $(p + 1)$ संख्या में संकेंद्रित रिंग होते हैं। ϕ वह दिगंशीय कोण है जो स्व-उपचार गुणों को दिखाता है जैसा कि एक बेसेल-गॉसियन किरण समान परिस्थितियों में करता है लेकिन उनसे अधिक दूर तक प्रसारित होता है।

साहित्य में इन घटनाओं के बारे में कई अध्ययन मौजूद हैं। हालाँकि, उनमें से अधिकांश लेजरों से जुड़े हैं जिनमें OAM नहीं होता है, जैसे कि गॉसियन, सुपर-गॉसियन और क्यू-गॉसियन लेजर। सुरंग आयनित गैसों में गॉसियन किरण की तुलना में सुपर-गॉसियन लेजर किरण में अधिक विवर्तन विचलन पाया गया है। साहित्य यह भी दर्शाता है कि कुछ शोध ने बेसेल-गॉसियन किरण और लैगुएरे-गॉसियन किरण को संबोधित किया है। यह देखा गया है कि लैगुएरे-गॉसियन किरण, बेसेल किरण की तुलना में आगे फैल सकते हैं और समान प्रारंभिक स्थितियों के तहत अधिक मजबूती दिखाते हैं। हालाँकि, ये अध्ययन मुख्य रूप से स्थानिक विकास पर ध्यान केंद्रित करते हैं और केवल एक प्रकार की गैर-रैखिकता पर विचार करते हैं। इसके अलावा, LG लेजर के स्थानिक-समय (spatio-temporal) विकास पर चर्चा नहीं की गई है, जो प्लाज्मा माध्यम से फैलने के दौरान स्पंद की तीव्रता और चरण भिन्नता का एक आंतरिक दृश्य प्रदान करता है।

इस शोध प्रबंध में हमने कम सघन प्लाज्मा में कक्षीय कोणीय गति ले जाने वाले लेजर के स्थानिक-समय विकास की प्रसार विशेषताओं की जांच की है और स्पंद स्व-केन्द्रन और स्व-संपीड़न पर लेजर के OAM के प्रभावों की व्याख्या की है। शुरु में LG लेजर के स्थानिक रूपरेखा के विकास पर सापेक्षतावादी और पॉंडरोमोटिव गैर-रैखिकता की एक साथ उपस्थिति के प्रभावों का अध्ययन किया गया है। फिर, हमने केवल

सापेक्षतावादी गैर-रैखिकता पर विचार करते हुए LG लेजर के स्थानिक-समय विकास की जांच की। अंततः हमने क्रमशः गैर-चुंबकीय और चुंबकीय प्लाज्मा में LG लेजर के सापेक्षतावादी आवृत्ति स्थानांतरण पर ध्यान केंद्रित किया। गणितीय मॉडल के रूप में, जहां हमने तरंग समीकरण को हल करने के लिए WKB दृष्टिकोण पर विचार किया है, फिर धीरे-धीरे बदलते आवरण सन्निकटन (SVE) और इकोनालाइज़ेशन का उपयोग करके हमने लेजर किरण की चौड़ाई और स्पंद अवधि के लिए अंतर समीकरण निकाले हैं। हमने वह स्थिति भी प्राप्त की है जहाँ विभिन्न अरैखिकताएँ एक दूसरे को रद्द कर देती हैं, और लेजर स्पंद माध्यम से प्रसारित होने के दौरान अपना आकार बनाए रखता है। फिर MATLAB सॉफ्टवेयर का उपयोग करके रनगे-कुट्टा 4वें क्रम (Runge-Kutta 4th order) विधि का उपयोग करके अंतर समीकरणों को संख्यात्मक रूप से हल किया जाता है। परिणामों को विभिन्न संख्यात्मक मापदंडों के लिए आलेखित किये गये हैं और वक्रों के व्यवहार में भिन्नता का अध्ययन किया गया है।

Table of Contents

Certificate	i
Acknowledgements	iii
Abstract	v
List of Figures	xv
List of Symbols	xix
Chapter 1: Introduction and Literature Review	1
1.1 Laser-Plasma Interaction	1
1.1.1 Various Nonlinearities.....	2
1.1.2 Various Nonlinear Phenomena.....	3
1.2 Laser Carrying Orbital Angular Momentum (OAM)	6
1.2.1 Generation of Orbital Angular Momentum.....	6
1.2.2 Applications of OAM Beam	7
1.3 Laguerre-Gaussian (LG) Beams.....	8
1.4 Methodology and Mathematical Techniques.....	9
1.4.1 Paraxial Approximation	11
1.4.2 Moment Theory.....	11
1.4.3 Variational Approach.....	12
1.5 Literature Review	12
1.6 Motivation	14
1.7 Structure of the Thesis.....	15
Chapter 2: Effect of Relativistic and Ponderomotive Nonlinearities on the Propagation Characteristics of Pure Radial Mode of Laguerre-Gaussian Laser	21
2.1 Introduction	21
2.2 Mathematical Formalism.....	22
2.2.1 Paraxial Wave Equations for Laguerre-Gaussian Beam	22
2.2.2 Evaluation of Nonlinear Effective Dielectric Function.....	24
2.3 Numerical Results and Discussion	26
2.4 Conclusions	32
Chapter 3: Propagation of Twisted Laser Carrying Orbital Angular Momentum in Magnetized Plasma	33
3.1 Introduction	33
3.2 Analytical Scheme.....	34
3.3 Numerical Analysis and Results.....	37

3.4	Conclusions	43
Chapter 4: Spatio-Temporal Evolution of Twisted Laguerre-Gaussian Laser in Magnetized Plasma		45
4.1	Introduction	45
4.2	Mathematical Formalism.....	46
4.2.1	Derivation of Nonlinear Dielectric Constant.....	49
4.2.2	Critical Conditions	49
4.3	Numerical Results and Discussions.....	50
4.4	Conclusions	59
Chapter 5: Relativistic Frequency Shifting of Laser Carrying Orbital Angular Momentum in an Unmagnetized Plasma.....		61
5.1	Introduction	61
5.2	Mathematical Background.....	61
5.3	Numerical Results and Discussions.....	64
5.4	Conclusions	66
Chapter 6: Relativistic Frequency Shifting of Laser Carrying Orbital Angular Momentum in a Magnetized Plasma.....		67
6.1	Introduction	67
6.2	Mathematical Formalism.....	67
6.3	Numerical Results and Discussions.....	70
6.4	Conclusions	75
Chapter 7: Conclusions, Applications and Scopes for Future.....		77
7.1	Conclusions of Thesis Work.....	77
7.2	Applications of the Results.....	79
7.3	Scopes for Future.....	79
References		81
Brief Biodata of the Author		89

List of Figures

FIG. 1.1. Ponderomotive force exerted by laser.

FIG. 1.2. (a) Different nonlinearities behind self-focusing, (b) Ponderomotive self-focusing of laser in plasma.

FIG 1.3. Helical phase structure of LG laser for different values of l .

FIG 1.4. Intensity profile of LG beam for different values of l and p .

FIG. 2.1. Normalized radius, $\rho = \frac{r_0 \omega_{p0}}{c}$, as a function of normalized initial intensity, a_0^2 , of the laser for critical condition when nonlinearity balances the diffraction effect.

FIG. 2.2. Laser beam width parameter as a function of distance of propagation, $\xi = \frac{z}{R_d}$, for different initial laser beam intensities $a_0^2 = 0.050, 0.0564$ and 0.070 with $\rho = 2.5, r_0 = 30 \times 10^{-4}$ cm, $\omega = 2 \times 10^{16}$ Hz and $\omega_{p0} = \rho \frac{c}{r_0}$.

FIG. 2.3. Laser beam width parameter as a function of distance of propagation, $\xi = \frac{z}{R_d}$ for different dimensionless beam radii $\rho = 1.0, 1.2980, 2.0$ and 4.0 with $a_0^2 = 0.07, r_0 = 30 \times 10^{-4}$ cm, $\omega = 2 \times 10^{16}$ Hz and $\omega_{p0} = \rho \frac{c}{r_0}$.

FIG. 2.4. Radial and axial distribution of normalized intensity and plasma density for self-focusing condition with $a_0^2 = 0.07, \rho = 2.5, r_0 = 30 \times 10^{-4}$ cm and $\omega = 2 \times 10^{16}$ Hz.

FIG. 2.5. Radial and axial distribution of normalized intensity and plasma density for defocusing condition with $a_0^2 = 0.05, \rho = 2.5, r_0 = 30 \times 10^{-4}$ cm and $\omega = 2 \times 10^{16}$ Hz.

FIG. 3.1. The transverse intensity profile of the Laguerre-Gaussian laser for different values of orbital angular momentum (l).

FIG. 3.2. Variation of equilibrium beam radius (self-trapped mode) with respect to (a) initial intensity for the fixed $\omega_c = 0.1\omega$ and (b) to cyclotron frequency for fixed $a_0^2 = 0.06$ for LCP and RCP lasers with $l = 1$. $\omega_p = 0.6\omega$ is taken as another parameter.

FIG. 3.3. Evolution of the laser beam width parameter with respect to the propagation distance (normalized) for left and right circularly polarized Laguerre-Gaussian (LG_{pl}) lasers, when a static magnetic field ($\omega_c = 0.1\omega$) is applied in the medium provided the initial intensity of the laser $a_0^2 = 0.06$, plasma frequency $\omega_p = 0.6\omega$, $\frac{r_0\omega}{c} = 10$, and $l = 1$.

FIG. 3.4. Evolution of the laser beam width parameter with respect to the propagation distance (normalized) for different cyclotron frequencies ($\omega_c = 0, 0.1\omega, 0.15\omega, 0.2\omega$), provided the initial intensity of the laser $a_0^2 = 0.06$, $\frac{r_0\omega}{c} = 8$, $l = 1$, and $\omega_p = 0.6\omega$.

FIG. 3.5. Variation of (a) relativistic factor, (b) linear dielectric constant and (c) nonlinear dielectric constant with distance of propagation for different cyclotron frequencies ($\omega_c = 0, 0.1\omega, 0.15\omega, 0.2\omega$), provided $a_0^2 = 0.06$, $l = 1$, $\omega_p = 0.6\omega$, and $\frac{r_0\omega}{c} = 8$.

FIG. 3.6. Variation of (a) equilibrium beam radius with respect to the initial intensity, and (b) the laser beam width parameter with respect to the propagation distance (normalized) for different topological charge (OAM): $l = 0, 1, 2, 3$, provided $a_0^2 = 0.06$, $\frac{r_0\omega}{c} = 8$, $\omega_p = 0.6\omega$, and $\omega_c = 0.05\omega$.

FIG. 3.7. Variation of (a) relativistic factor, (b) linear dielectric constant and (c) nonlinear dielectric constant with distance of propagation for different topological charge (OAM): $l = 0, 1, 2, 3$, provided $a_0^2 = 0.06$, $\omega_c = 0.05\omega$, $\omega_p = 0.6\omega$, and $\frac{r_0\omega}{c} = 8$.

FIG. 3.8. (a) Laser intensity (a^2), and (b) modified plasma density ($\frac{n_e}{n_0}$) at different distance of propagation for LG_{01} when $a_0^2 = 0.06$, $\omega_c = 0.1\omega$, $\omega_p = 0.6\omega$, and $\frac{r_0\omega}{c} = 8$.

FIG. 4.1. Temporal variation of Different chirped profiles of the Laser pulse. $\omega(\tau) = \omega_0(1 + b \tanh(\tau/s))$. (a) $b = -0.3$ (negatively chirped), (a) $b = 0$ (unchirped) (c) $b = 0.3$ (positively chirped).

FIG. 4.2. (a) ρ_0^{-2} vs. a_0^2 and (b) $\omega_0^{-2}\tau_0^{-2}$ vs. a_0^2 for different values of $l = 1, 2, 3, 4$, and 5 for $b = 0$ (unchirped laser). (c) ρ_0^{-2} vs. a_0^2 and (d) $\omega_0^{-2}\tau_0^{-2}$ vs. a_0^2 for different chirping conditions, $b = -0.3$ (negatively chirped), 0 (unchirped), and 0.3 (positively chirped) for LG_{01} laser at $\tau = -(1/2)$ * FWHM (front of the pulse). Given: $\omega_p = 0.6 \omega_0$ and $\omega_c = 0.1 \omega_0$, $s = 50$, $\tau_0 = 100 fs$.

FIG. 4.3. Variation of laser (a) spot size, f , (b) pulse width, g , and (c) group velocity, v_g , for different chirping conditions with chirping parameter $b = -0.3$ (negatively chirped) (solid blue curve), $b = 0$ (unchirped) (dashed red curve) and $b = 0.3$ (positively chirped) (dotted yellow curve). Given, $\Omega = 1 + b \tanh(\tau/s)$ with $s = 50$, $\omega_p/\omega_0 = 0.6$, $\omega_c/\omega_0 = 0.1$, $\tau_0 = 100$ fs, $a_0^2 = 10$, $l = 1$, $r_0\omega_0/c = 10$.

FIG. 4.4. Variation of laser (a) spot size (f), and (b) pulse width (g), (c) $\epsilon_{2\eta}$, (d) $\epsilon_{2\tau}$, and (e) group velocity v_g throughout the pulse, and (f) spatio-temporal profile of the LG laser at $z = 141.67 \mu\text{m}$, for different laser topological charge $l = 1, 2, 3, 4$ and 5 . Given the laser pulse is chirped with $\Omega = 1 + b \tanh(\tau/s)$, where $s = 50$, chirping parameter $b = 0.3$ (positively chirped), $\omega_p/\omega_0 = 0.6$, $\omega_c/\omega_0 = 0.1$, $\tau_0 = 100$ fs, $a_0^2 = 10$, $r_0\omega_0/c = 10$.

FIG. 4.5. Variation of laser (a) spot size (f), (b) pulse width (g), and (c) Group velocity (v_g) throughout pulse, and (d) spatio-temporal profile of the LG laser at $z = 120 \mu\text{m}$, for different laser intensity $a_0^2 = 4, 6, 8$, and 10 . Given the laser pulse is chirped with $\Omega = 1 + b \tanh(\tau/s)$, where $s = 50$, chirping parameter $b = 0.3$ (positively chirped), $\omega_p/\omega_0 = 0.6$, $\omega_c/\omega_0 = 0.1$, $\tau_0 = 100$ fs, $a_0^2 = 10$, $l = 1$, $r_0\omega_0/c = 10$.

FIG. 4.6. Variation of laser (a) spot size, f and (b) pulse width, g , (c) spatio-temporal profile of the LG laser at $z = 78.84 \mu\text{m}$, and (d) spatio-temporal profile of the LG laser for minimum g , for different laser pulse width $\tau_0 = 50$ fs, 100 fs, and 150 fs. Given the laser topological charge $l = 1$ with initial intensity $a_0^2 = 10$, chirped frequency $\Omega = 1 + b \tanh(\tau/s)$, where $s = 50$, chirping parameter $b = 0.3$ (positively chirped), $\omega_p/\omega_0 = 0.6$, $\omega_c/\omega_0 = 0.1$, $a_0^2 = 10$, $l = 1$, $r_0\omega_0/c = 10$.

FIG. 5.1. Frequency shifting with distance of propagation for different intensities of the laser (LG_{01}), $a_0^2 = 5, 7$, and 10 .

FIG. 5.2. Frequency shifting with distance of propagation for laser with different OAM, $l = 1, 2, 3, 4$ and 5 . Given, $a_0^2 = 10$, $\omega_p/\omega_0 = 0.6$, $r_0\omega_0/c = 10$, $\tau_0 = 100$ fs.

FIG. 5.3. Frequency shifting with distance of propagation for lasers with different pulse duration, $\tau_0 = 50$ fs, 100 fs, and 150 fs.

FIG. 6.1. Geometry of right- and left-handed circularly polarized waves propagating along Magnetic field.

FIG. 6.2. Spatio-temporal Variation of spot size and pulse duration for $\omega_c = 0.1\omega$, 0.2ω and 0.3ω . Polarization: RCP, $l = 1$, $a_0^2 = 10$, $\rho = 10$.

FIG. 6.3. Variation of beam width (f) and pulse duration (g) parameters at laser frontside ($T = -1.0$) with propagation distance for different magnetic field $\frac{\omega_c}{\omega_0} = 0.1, 0.2$ and 0.3 .

FIG. 6.4. Frequency shifting for different $\omega_c = 0.1\omega_0$, $0.2\omega_0$ and $0.3\omega_0$. Polarization: RCP, $l = 1$, $a_0^2 = 10$, $\rho = 10$, $\omega_p = 0.6\omega_0$, $\omega_0 = 3 \times 10^{14}Hz$, $\tau_0 = 100fs$.

FIG. 6.5. Frequency shifting at different locations $z = 50 \mu m$, $100\mu m$, and $150 \mu m$ for both RCP and LCP type polarization. $l = 1$, $a_0^2 = 10$, $\rho = 10$, $\omega_c = 0.1\omega_0$, $\omega_p = 0.6\omega_0$, $\omega_0 = 3 \times 10^{14}Hz$, $\tau_0 = 100fs$.

List of Symbols

\vec{A} : Complex amplitude of electric field amplitude of laser

\vec{B} : Magnetic field of laser

\vec{E} : Electric field of laser

\vec{F}_p : Ponderomotive force

\vec{F}_s : Electrostatic force due to charge separation

L : Finite plasma size/characteristic length of plasma

T_e : Temperature of electrons

a : Normalized electric field amplitude

c : Speed of light

c_s : Sound/acoustic speed

e : Electronic charge

ϵ_0 : Linear part of dielectric constant

ϵ_2 : Nonlinear part of dielectric constant

$\epsilon_{2\eta}$ and ϵ_{2t} : Nonlinear part of dielectric constant

ϵ : Dielectric constant of plasma

f : Beam width parameter of the laser

g : Pulse duration parameter of the laser

γ : Relativistic factor or Lorentz factor

l : Orbital angular momentum of laser

λ_D : Debye length

m_e : Mass of electrons

n_{cr} : Critical density of plasma electrons

n_{e0} , or n_0 : Electron density in plasma/background density of electrons

ν : Collisional frequency

ω_p : Plasma frequency

p : Radial index of Laguerre Gaussian laser

ϕ : Electric potential

ϕ_p : Ponderomotive potential

ϕ_s : Space charge potential

r : Radial coordinate

r_0 : Beam waist of the laser

v_g : Group velocity of laser

x : Distance

ξ : Normalized distance

z : Space coordinate